

Entanglement Transitions in Unitary Circuit Games

Raúl Morral-Yepes,¹ Adam Smith,^{2,3} S. L. Sondhi,⁴ and Frank Pollmann^{1,5}

¹*Technical University of Munich, TUM School of Natural Sciences, Physics Department, Lichtenbergstr. 4, 85748 Garching, Germany*

²*School of Physics and Astronomy, University of Nottingham, Nottingham, NG7 2RD, UK*

³*Centre for the Mathematics and Theoretical Physics of Quantum*

Non-Equilibrium Systems, University of Nottingham, Nottingham, NG7 2RD, UK

⁴*Rudolf Peierls Centre for Theoretical Physics, University of Oxford, Oxford, UK*

⁵*Munich Center for Quantum Science and Technology (MCQST), Schellingstr. 4, 80799 München, Germany*

Repeated projective measurements in unitary circuits can lead to an entanglement phase transition as the measurement rate is tuned. In this work, we consider a different setting in which the projective measurements are replaced by dynamically chosen unitary gates that minimize the entanglement. This can be seen as a one-dimensional unitary circuit game in which two players get to place unitary gates on randomly assigned bonds at different rates: The “entangler” applies a random local unitary gate with the aim of generating extensive (volume law) entanglement. The “disentangler”, based on limited knowledge about the state, chooses a unitary gate to reduce the entanglement entropy on the assigned bond with the goal of limiting to only finite (area law) entanglement. In order to elucidate the resulting entanglement dynamics, we consider three different scenarios: (i) a classical discrete height model, (ii) a Clifford circuit, and (iii) a general $U(4)$ unitary circuit. We find that both the classical and Clifford circuit models exhibit phase transitions as a function of the rate that the disentangler places a gate, which have similar properties that can be understood through a connection to the stochastic Fredkin chain. In contrast, the “entangler” always wins when using Haar random unitary gates and we observe extensive, volume law entanglement for all non-zero rates of entangling.

I. INTRODUCTION

Quantum many-body systems out of equilibrium represent a challenging frontier and have been shown to exhibit extremely rich phenomena. These include, for example, a dynamical phase transition between ergodic and many-body localized phases as a function of disorder strength [1–6], quantum many-body scars [7–10], and discrete time crystals that can occur in periodically driven systems [11–17]. All the above examples occur in closed quantum systems subject to unitary evolution.

A new perspective comes from the combination of unitary evolution of a quantum many-body system with measurements. In pioneering works [18–22], an entanglement phase transition was identified in the dynamics of circuits of random unitary gates interleaved with local projective measurements. This phase transition separates a disentangling phase obeying an area law from an entangling phase obeying a volume law. Successively, it has been shown that additional phase transitions between different symmetry broken and topological phases can occur within the area law phase [23–27].

In this paper, we consider a different setting in which the projective measurements are replaced by unitary gates that are dynamically chosen to disentangle the state. While finding the disentangling unitary requires certain knowledge about non-local properties of the state, the action of the unitary gate itself is local. We can interpret our approach as a (1+1)D circuit game of L sites in which two players get to place unitary gates on randomly assigned bonds at different rates: At each updating step, a random bond of the chain is chosen. With

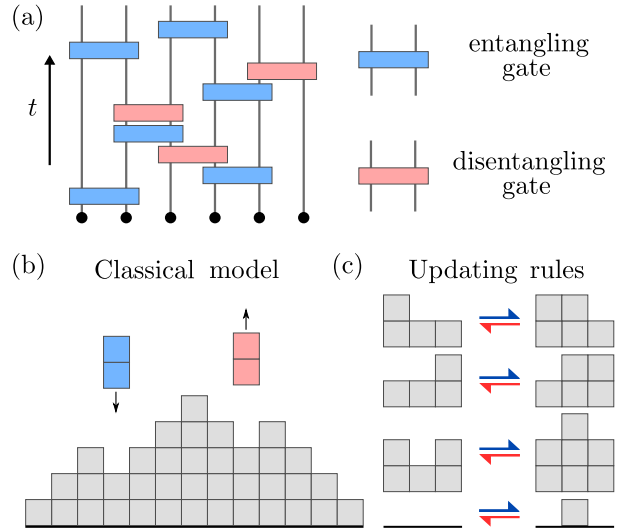


FIG. 1. (a) Illustration of the unitary circuit game: Blue boxes represent random unitary gates and red gates are unitary gates chosen to disentangle the bond. (b) Classical version of the circuit game as a surface growth model, where entangling and disentangling operations are substituted by adding or removing blocks in a lattice. (c) Updating rules of the classical model: The entangler (blue arrow) adds blocks and the disentangler (red arrow) removes them, with the constraint that the difference of heights between adjacent bonds is at most one and the height can’t be negative.

probability $1 - p$ the “entangler” acts with a random unitary and otherwise, with probability p , the “disentan-

gler” acts by minimizing the entanglement entropy on the given bond. Here we measure the entanglement entropy $S = -\text{Tr}\rho_A \ln \rho_A$ with the reduced density matrix ρ_A , where A includes all qubits left of the bond. A time step is defined to be a set of L updating steps. A possible realization of this model is depicted in Fig. 1a. This game has two simple limiting cases: For $p = 0$, only the entangler gets to play, resulting in a random-unitary circuit, which in turn leads to a volume law state [28]. For $p = 1$, the entanglement will remain zero at all times and thus yield an area law state. Here we are interested in the behavior of our model for intermediate values of $0 < p < 1$. Having defined the rules of the unitary circuit game, several questions naturally emerge: Is there a phase transition between the volume and area-law entanglement at finite p ? If so, what are its universal properties?

We provide answers to these questions in several different variants of the game: In Sec. II, we start with a classical surface growth model for which the competition between entangling and disentangling gates is substituted by a competition between increasing and decreasing the height of a surface locally, as shown in Fig. 1b. Second, in Sec. III we investigate a Clifford circuit. In this case, finding the optimal disentangler amounts to selecting from the discrete set of two-qubit Clifford unitary gates. Finally, in Sec. IV, we consider general continuously parameterized unitary gates. The entangler chooses gates randomly from the Haar distribution, whereas the disentangler now involves the optimization of unitary gates on a given bond in order to minimize the bipartite entanglement entropy.

II. CLASSICAL MODEL

In this section, we study a surface growth model in (1+1)D that can be interpreted as a classical version of the unitary circuit game. We start by introducing the update rules defining the model. We then numerically study the phase transition that occurs by tuning the disentangling rate. Finally, we show that this model is closely related to a stochastic Fredkin spin chain [29].

For our classical surface growth model, a bond (block) is chosen uniformly at random, and then either the entangler or disentangler takes their go with probability $1 - p$ and p , respectively. That is, p controls the disentangling rate. When the entangler is selected, the evolution of the height surface follows the dynamical rule

$$\begin{aligned} &\text{Entangler (probability } 1 - p): \\ &S(x, t + \Delta t) = \min\{S(x - 1, t), S(x + 1, t)\} + 1, \end{aligned} \quad (1)$$

where x is the bond index, t denotes the time, and $\Delta t = 1/L$. When the disentangler is selected, the evolution follows the dynamical rule

$$\begin{aligned} &\text{Disentangler (probability } p): \\ &S(x, t + \Delta t) = \max\{S(x - 1, t), S(x + 1, t), 1\} - 1, \end{aligned} \quad (2)$$

where the one in the argument of the max-function is added to preserve the $S(x, t) \geq 0$ constraint for all times, i.e., the height can’t be negative.

The combination of the above rules then defines our classical entangling-disentangling game, as depicted in Fig. 1b: at each updating step a random bond is chosen and with probability p the bond is disentangled following Eq. (2) or with probability $1 - p$ the bond is entangled with Eq. (1). We can interpret this as a (1+1)D surface growth/depletion model, where the height of each bond corresponds to the entanglement entropy of that bipartition. The only constraints are that the height cannot be negative and the difference in height between two adjacent bonds can be at most one.

A. Numerical results

The limiting cases of this model can be easily understood: For $p = 0$ the disentangler does not act and thus at large times the system reaches a pyramid shaped steady state. The increase of height from a flat initial state is described by KPZ universal scaling, as derived in Ref. [28], where this model was introduced to study entanglement growth in Haar random unitary circuits. The limit $p = 1$ has a flat steady state, with height 0 at every site. Below we investigate the transition between these two limiting cases.

The classical model can be efficiently simulated numerically, allowing us to reach large system sizes, up to $L = 8192$. For each value of the “disentangler” probability p and system size L that we consider, we run 10^3 different realizations of the circuit (except at the critical point $p_c = 1/2$, where we run 10^4 realizations). At each realization, we evolve the system until the dynamical steady state is reached, and then evolve for extra 10^5 time steps in which we average over the quantities that we are interested in. Note that throughout this paper, all quantities are understood to be averaged in the steady state of the system, unless otherwise specified.

Figure 2a shows the half-chain height $S_{L/2}(p, L)$, as a function of L for several disentangling probabilities p across the phase transition. We identify three different behaviors: For $p < p_c$ we find a *volume law* phase, where the height increases linearly with system size. Note that in the thermodynamic limit, all the lines in this phase converge to the line $S_{L/2} = L/2$. For $p > p_c$ we find an *area law* phase, where the average height converges to a constant independent of system size. Finally, at the critical point $p_c = 1/2$ the height is proportional to the square root of system size. These numerical results strongly suggest a phase transition between volume and area law phases.

To further characterize the different phases, we study the averaged fluctuations around the average steady state

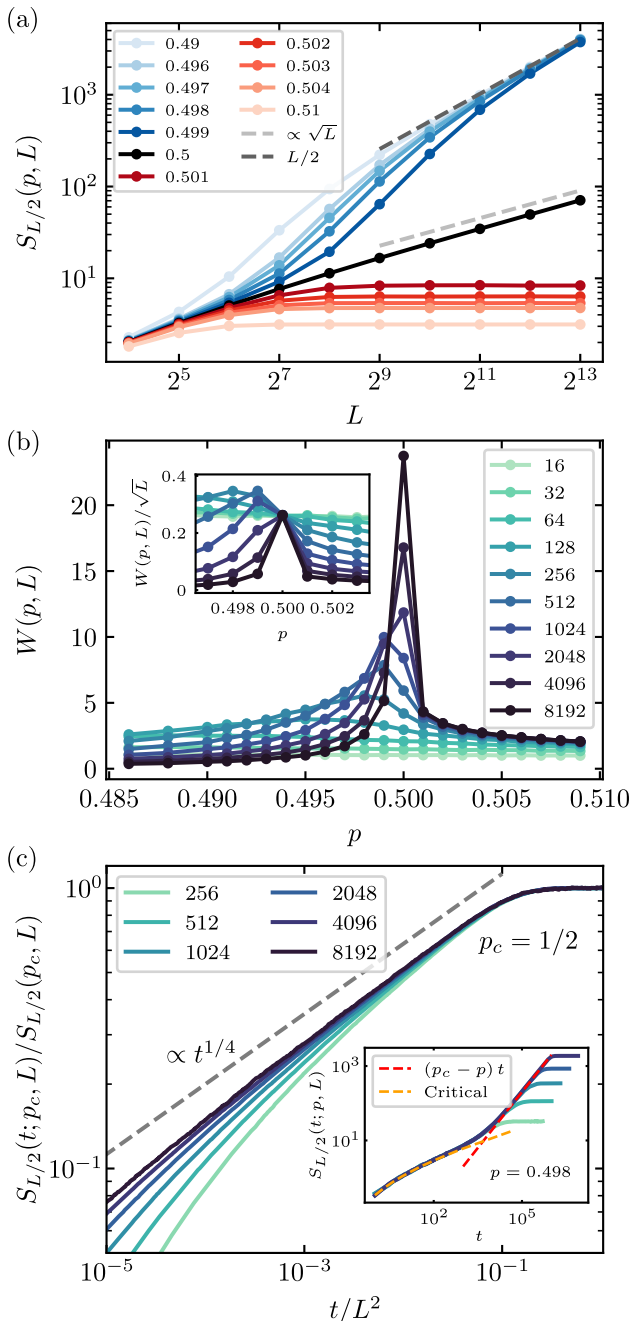


FIG. 2. (a) Half-chain height as a function of system size L for different values of the disentangling probability p . (b) Spatial fluctuations $W(p, L)$ as a function of the disentangling probability p across the phase transition for different system sizes L . The inset shows $W(p, L)/\sqrt{L}$, that takes a positive value (independent of system size) at the critical point and tends to zero otherwise. (c) Time evolution, averaged over 10^4 realizations, of the half-chain height normalized by the steady state value as a function of t/L^2 at criticality, $p_c = 1/2$. The height increases as a power law with exponent $\beta = 1/4$. The inset shows the time evolution of $S_{L/2}$ at $p = 0.498$ (in the volume law phase) for several values of L . For $t < t_c$ the evolution is critical (orange line), while for $t > t_c$ the height increases linearly with t (red line).

height profile of the system using the quantity

$$W(p, L) = \left(\frac{1}{L} \sum_{x=1}^L \left(S(x, p, L) - \overline{S(x, p, L)} \right)^2 \right)^{1/2}, \quad (3)$$

where the overline indicates the average of the quantity in the steady state. The quantity $S(x, p, L)$ is a stochastic realization of the height profile in the steady state at bond x , for disentangling probability p and systems size L . In practice, we take t much greater than the relaxation time to the steady state, and average over time. The spatial fluctuations $W(p, L)$ in the classical model are shown in Fig. 2b as a function of p and L . In the volume law phase the relative fluctuations tend to zero as the system size is increased, since only in a finite region around the center of the system there will be height variations. In the language of stochastic dynamics, this corresponds to an inactive phase. In the area law phase, fluctuations converge to a constant value for sufficiently large system sizes, indicating an active phase, where fluctuations are equal at every point in the bulk of the system. At the critical point, we have a strongly fluctuating phase, where fluctuations increase with system size as \sqrt{L} , as shown in the inset of Fig. 2b.

Finally, we focus on the dynamics of the system and its thermalization time in the critical point $p_c = 1/2$. In particular, we study how the steady state is reached by starting from a flat state with zero height at all sites. Figure 2c shows the evolution of the half-chain height averaged over 10^4 trajectories, normalized by the steady state value. The increase of the half-chain height follows a power-law in time, $S_{L/2}(t; p_c, L) \propto t^\beta$, with an exponent $\beta = 1/4$, so that the equilibration time in this phase is $T_{\text{eq}} \propto L^z$, with dynamic exponent $z = 2$. Moreover, we find that the dynamic exponent $z = 0$ in the area law phase and $z = 1$ in the volume law phase, respectively. In the inset of Fig. 2c we show the time evolution of the half-chain entanglement entropy for a disentangling probability in the volume law phase but close to criticality. We distinguish two regimes: For $t < t_c$, the evolution is the same as in the critical point, i.e. approaching $t^{1/4}$. Instead, for $t > t_c$, the height increases as $(1/2 - p)t$, linearly in time. The critical time t_c , where the evolution changes its behavior, is fixed by the intersection of the two lines. When approaching the critical point it diverges as a power law,

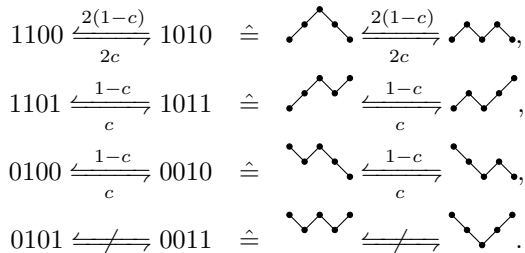
$$t_c \sim (p_c - p)^{-4/3}, \quad (4)$$

with critical exponent $4/3$.

B. Comparison with Fredkin chain results

The transition in our classical model can be understood through a connection to the stochastic classical Fredkin chain [29], a model originally proposed as an example of a power law violation of the area law in quantum spin

chains [30–33]. The stochastic Fredkin model is defined on a chain of L sites and each site can be either empty or occupied by a particle ($z_i = 0, 1$). We focus on the case with $L/2$ particles, i.e. $\sum_i z_i = L/2$. This model can be interpreted as a height model by defining the bond variable $h_n = \sum_{i=1}^n (2z_i - 1)$, with the condition that $h_n > 0$ for every n . The evolution of the model follows a continuous-time Markov chain evolution, with a parameter c that captures the rate at which transformations occur. In particular, the evolution is described by the following updating rules:



Note that these rules avoid the creation of states of the form 0011, which could lead to negative heights.

While this model looks similar to the model we have introduced, there are a few key differences: First, in our classical model, the rate at which the transformations happens is not fixed by a single parameter, but instead depends on the state of the system. For example, the probability of the disentangler to act is proportional to the number of bonds at which it is possible to reduce the height. Second, the Fredkin chain dynamics are described by a continuous-time Markov process, in contrast to the discrete dynamics of our model. Third, the Fredkin model does not allow flat regions, i.e., neighboring sites with the same height. This is allowed in our model, but they are only created at zero height. These flat regions are irrelevant in the volume law phase in the thermodynamic limit.

While these differences lead to differing dynamics in the two models, the steady states agree at the critical point $c = p_c = 1/2$. Indeed, the difference between continuous and discrete time becomes irrelevant for the average properties of the steady state. Furthermore, we can understand the critical point as approached from the volume law side where flat regions are irrelevant, and the critical point corresponds to an equilibrium between entangling and disentangling operations.

The connection to the Fredkin chain is supported by our numerical simulations. The numerically observed scaling of the height with \sqrt{L} at the critical point agrees with analytical results for the Fredkin chain (given by an average of Dyck paths). Additionally, the critical profile of our model converges to the analytical result for the Fredkin chain, which is given by [34]

$$\overline{S(x, L)} = \frac{4}{\sqrt{2\pi}} \sqrt{\frac{x(L-x)}{L}}, \quad (5)$$

(with an extra factor of 2 with respect to the equation

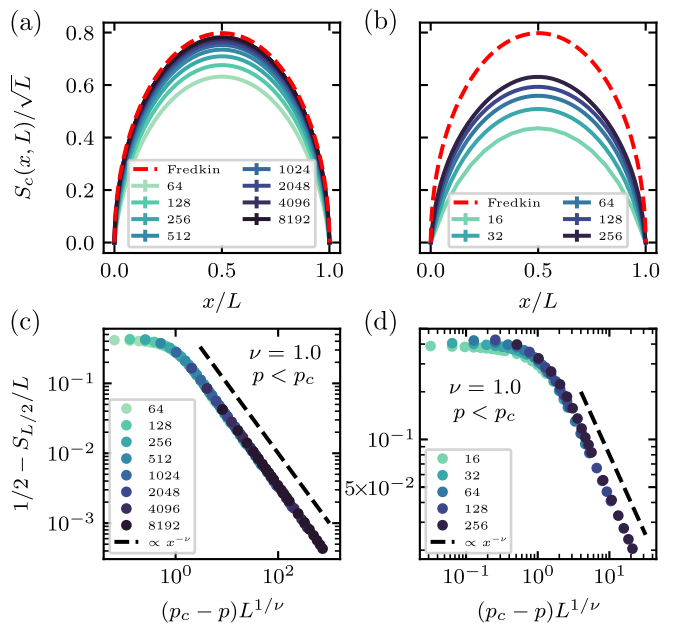


FIG. 3. (a) Steady state averaged profile at criticality, $p_c = 1/2$, of the classical model for various system sizes, normalized by \sqrt{L} . The dashed red line indicates the analytic result for the Fredkin chain in the thermodynamic limit. (b) Steady state averaged profile at criticality, $p_c = 0.382$, of the Clifford model. (c) Finite size scaling of the half-chain height normalized by the system size L when approaching the critical point from the volume law phase. The critical exponent $\nu = 1$ corresponds to the analytic result in the stochastic Fredkin spin chain. (d) Finite size scaling of the half-chain entanglement entropy in the Clifford model normalized by the system size L when approaching the critical point from the volume law phase, with approximate critical exponent $\nu = 1.0$.

in [34], since there they consider jumps of $1/2$ instead of 1) as depicted in Fig. 3a. From a finite size scaling analysis of the half-chain height normalized by the system size, we obtain that the critical exponent for the correlation length when approaching the critical point from the volume law phase is $\nu = 1$, as shown in Fig. 3c. This coincides with the analytical results for the Fredkin chain, where the correlation length scales as [29]

$$\xi = \ln \left(\frac{c}{1-c} \right)^{-1} \propto |c - 1/2|^{-1}. \quad (6)$$

III. CLIFFORD MODEL

As a first quantum model, we consider unitary circuits that are restricted to Clifford gates [35]. While simulating general quantum circuits on classical computers is a difficult task, Clifford circuits can be efficiently simulated using stabilizer states [36–39]. Clifford circuits offer a sufficiently broad set of operations to show interesting behavior, while keeping the complexity polynomial with

system size. In fact, Clifford circuits have been the main playground to study measurement-induced phase transitions [18, 19, 21]. The group of Clifford unitaries acting in two qubits is a finite group (containing 11520 unitaries), and therefore finding the optimal unitary to disentangle a bond can be achieved by trying all unitaries until one is able to maximally disentangle the given bond. Moreover, the entanglement entropy in the stabilizer states generated by Clifford circuits is always an integer in units of $\log(2)$, and therefore the height picture of the classical model translates to this case, changing the height by the bipartite entanglement. However, the rules for entangling and disentangling are more complicated in the Clifford case as compared to the classical model.

In the Clifford model, we consider a chain of L spin-1/2 degrees of freedom (qubits) with open boundary conditions. This chain is evolved as depicted in Fig. 1a. The entangling gates are drawn randomly and uniformly from the discrete set of Clifford unitary gates, and the disentangling gates are appropriately chosen Clifford unitary gates that maximally reduce the entanglement on that bond. This model has several key differences compared to the classical one: First, the entangler in this case is not necessarily optimal. Since it only applies a random Clifford unitary, there is a finite probability that it does not increase the entanglement or even that it disentangles the bond. Second, the disentangler is not always able to reduce the entanglement as much as it is allowed by rule Eq. (2). However, it is always fulfilled that the disentangler at least reduces the entanglement to match that of the adjacent bonds, i.e. $S(x, t+1) \leq \max\{S(x-1, t), S(x+1, t)\}$.

The disentangling step can be simplified by first looking at the value of the entanglement entropy on adjacent bonds: if $S(x, t) < \min\{S(x-1, t), S(x+1, t)\}$, then that bond cannot be further disentangled due to sub additivity. Otherwise, one has to try unitaries in the Clifford group until one of them is able to maximally disentangle the bond. We numerically find that it is sufficient to choose the disentangling gate from a subset of 19 Clifford unitaries to maximally disentangle any given bond. This minimal set of unitaries is not unique, however, the phase transition that we describe in the following is not affected by the choice, see App. A for a discussion about different disentangling methods.

A. Numerical results

Since the numerical simulations of this model are more demanding than the ones of the classical model, we are limited to system sizes up to $L = 256$. The numerical results show a phase transition between a volume law and an area law phase located at $p_c \approx 0.382$, as shown in Fig. 4a. The reduction of p_c with respect to the classical model is, in part, caused by the entangler applying random Clifford unitary gates that may not be optimally increasing the entanglement or that could even reduce it.

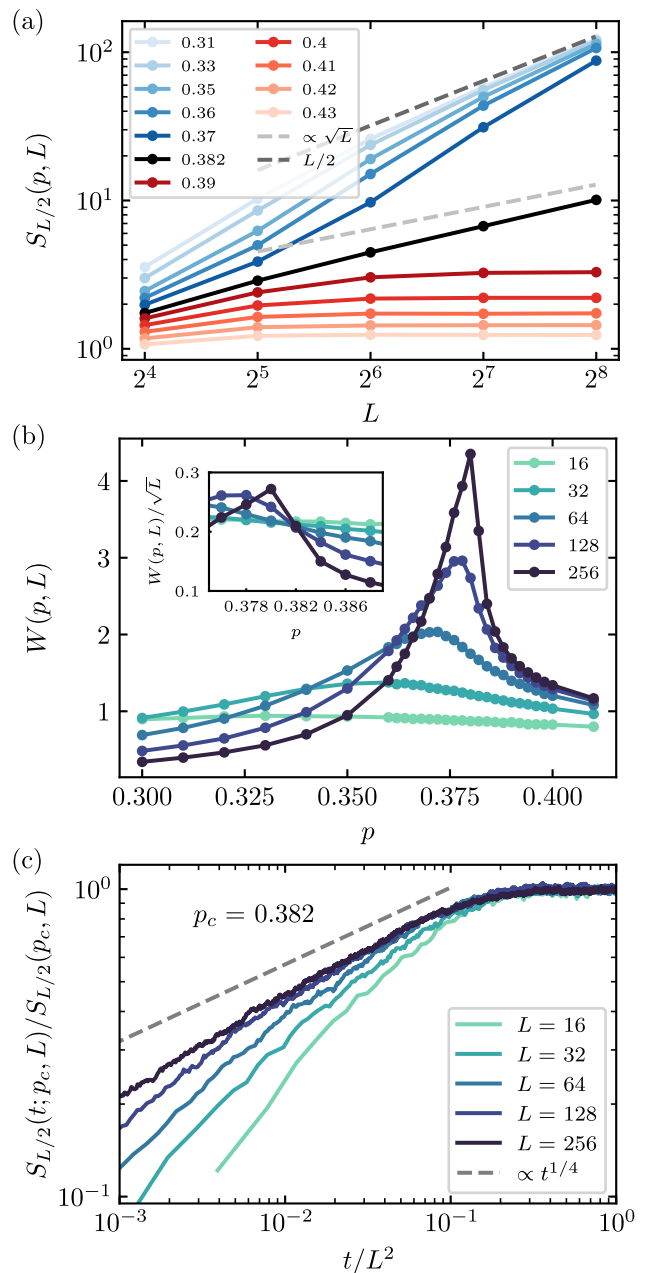


FIG. 4. (a) Half-chain entanglement entropy $S_{L/2}(p, L)$ as a function of system size L for different values of the disentangling probability p . (b) Spatial fluctuations $W(p, L)$ as a function of the disentangling probability p across the phase transition for different system sizes L . The inset shows $W(p, L)/\sqrt{L}$, which takes a positive value (independent of system size) at the critical point. (c) Time evolution of the half-chain height as a function of time at criticality, $p_c = 0.382$, circuit averaged over 10^3 realizations. The height increases as a power law with exponent $\beta \approx 1/4$, with dynamic exponent $z = 2$.

For $p < p_c$, the half-chain entanglement entropy asymptotically converges to $L/2$, while for $p > p_c$ it converges

to a constant value. The behavior at the critical point is similar to the classical case, scaling as \sqrt{L} . The limitation in system size and the large finite size effects (also present in the classical case) do not allow for a precise quantification of the scaling exponent with the numerical data available. Figure 4b shows the behavior of the spatial fluctuations as a function of the disentangler probability. The behavior is very similar to the one found for the classical model. The divergence of the spatial fluctuations at the critical point allows us to determine with better precision the location of the critical point (inset). Lastly, we investigate the time evolution of the entanglement entropy in the critical point, as shown in Fig. 4c. For sufficiently late times, the behavior of the evolution appears to converge to a power law with t , with an exponent close to $1/4$ as was the case in the classical model. Moreover, we find the same dynamic exponents of $z = 2$ in the critical phase, $z = 1$ in the volume law phase, and $z = 0$ in the area law phase.

The averaged profile in the steady state of the critical point is shown in Fig. 3b. The system sizes that can be reached by the numerical simulations are not sufficiently large to convincingly determine whether the profile is converging to one of the Fredkin chain, given by Eq. (5). However, we can see that even if the proportionality constant is not the same, the profile has qualitatively the same shape as the one in the classical case. Figure 3d shows the finite size scaling collapse for the half-chain entanglement entropy normalized by the system size. Based on the limited available data, we find that the critical exponent for the correlation length when approaching the critical point from the volume law is $\nu \approx 1$. Thus the exponent appears to be in agreement with the one found for the classical version of the game.

IV. HAAR RANDOM MODEL

We now study the circuit model in the most general case, where unitary gates are taken without restriction from the unitary group $U(4)$. While the minimization of the entanglement entropy in the Clifford case was straightforward by choosing a unitary from a discrete set, the disentangling in the Haar case is more challenging. In particular, we have to find an optimal unitary in $U(4)$ by tuning several continuous parameters—for the case of two site unitary gates, this implies that the disentangler has to perform a minimization with 16 continuous parameters of a function that is likely to exhibit many local minima. There exist different entanglement measures that quantify the amount of entanglement of a pure state and thus we have to choose one in order to perform the entanglement minimization. Here, we will focus on a bipartite von Neumann disentangler, i.e., a disentangler that minimizes the bipartite entanglement entropy S across the given bond [40]. In App. B, we discuss how the disentangler performs when trying to remove all the entanglement of a state generated by a depth $2L$ random

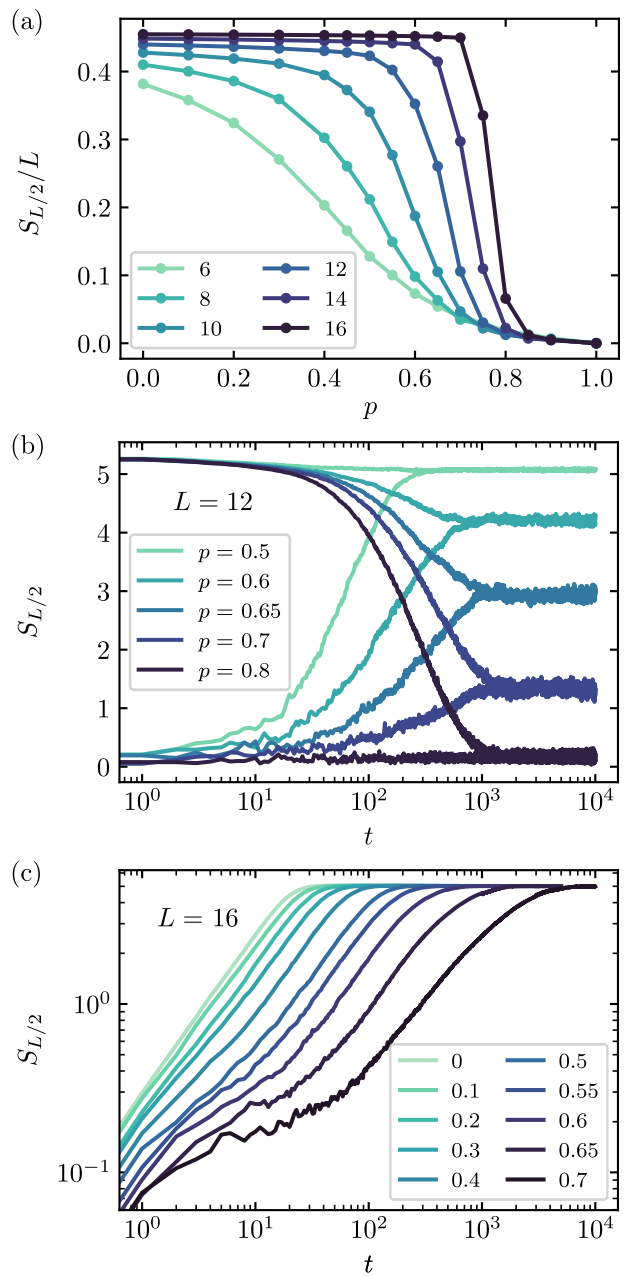


FIG. 5. (a) Order parameter $S_{L/2}/L$ versus the disentangler probability for increasing system size. (b) Time evolution of the half-chain entanglement entropy for fixed system size $L = 12$ starting from a product state and from a random Haar state, circuit averaged over 50 realizations. (c) Time evolution for system size $L = 16$ and increasing disentangling probabilities. Circuit averaged over 500 realizations until reaching the steady state for short times, and over 10 realizations after that.

circuit. We find that the disentangling time increases exponentially with system size.

To simulate the system, we rely on the numerically exact evolution of the full wavefunction of the system

and are thus limited to small system sizes, up to $L = 16$.

A. Numerical results

We first investigate the steady-state half-chain entanglement entropy divided by the system size, $S_{L/2}/L$. This quantity serves as an order parameter for the transition: in a volume law phase, this quantity converges to a finite value in the thermodynamic limit, while in an area law phase it goes to zero. Figure 5a shows this order parameter versus the disentangler probability p for the random Haar circuit with the von Neumann disentangler. As the system size is increased, the region in which the system reaches a maximally entangled state is enlarged, indicating that no phase transition exists for any disentangler probability $p < 1$. Therefore, in the thermodynamic limit any effort from the disentangler is futile: even an infinitesimal rate of random unitary gates is expected to eventually lead to a maximally entangled state.

Figure 5b shows the circuit averaged time evolution for fixed system size $L = 12$ and several different disentangling probabilities, starting from two different initial states: a product state and a Haar random state. We find that the steady state reached from both possible initial states is the same for any disentangling probability. Even though the disentangler cannot stabilize an area law phase, it does have an effect in delaying the time required to reach the equilibrium state. In Fig. 5c we fix system size $L = 16$ and check the time evolution for increasing disentangler probability p . The time required to achieve the steady state, which is a maximally entangled state, diverges as $p \rightarrow 1$. In fact, we find that when approaching $p = 1$, the equilibration time diverges faster than any power law in $1/(1-p)$ and instead is best described by an exponential divergence.

We are now going to provide a heuristic argument for the absence of an area law for $p < 1$, based on the creation of multipartite entanglement that the gate-based disentangler is unable to remove effectively. Let us first consider a simplified model in which we prepare a state by applying n_e random gates to an initial product state. Next, a disentangling circuit is applied until the total entanglement is reduced below a certain threshold. Figure 6 shows how the average number of disentangling gates n_d depends on n_e . For $n_e \ll L$, the unitaries applied to the system almost never overlap, such that there is no creation of any multipartite entanglement. In this case, the disentangler just needs to find the entangled bonds, and then the entanglement can be completely eliminated. The average time needed to disentangle can be analytically calculated in this limit, and it is given by $n_d(n_e) = (L-1)H_{n_e}$, where H_{n_e} is the n_e -th harmonic number, which coincides with our numerical results (inset Fig. 6). Instead, when $n_e \gtrsim L$ the overlapping gates lead to the creation of multipartite entanglement, making the disentangling task much harder. For a fixed depth of the entangling circuit, $n_e/L \gtrsim 1$, the depth of the disen-

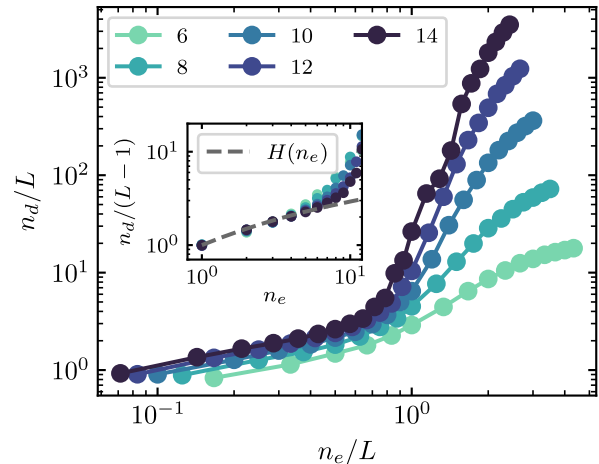


FIG. 6. Average number of disentangling steps n_d needed to disentangle a state created by a circuit of n_e randomly placed two-qubit unitary. The condition used to consider the state disentangled is that the sum of the bipartite entanglement at every bond satisfies $\sum_x S(x) < 10^{-3}L$. The inset shows the collapse for $n_e \ll L$ with $n_d(n_e)/L = H_{n_e}$, with H_n the n -th harmonic number.

tangling circuit required increases faster than linear with system size. In particular, as discussed in App. B, for $n_e/L = 2L$, the disentangling time grows exponentially in L — a property that we conjecture to hold for any $n_e/L \gtrsim 1$. In contrast, the circuit depth required by the entangler to create a maximally entangled state grows linearly with system size [28].

Now, we can turn to the unitary circuit game, where the gates that entangle and disentangle occur at a certain rate throughout the time evolution. For a disentangling rate p close to one, the entangler is initially not able to effectively generate entanglement, since there is a high probability that any random gate will be undone by a disentangling gate before the entangler can place another. Nevertheless, given enough time, there is a finite probability that the entangler is able to create a region of length l with multi-partite entanglement by overlapping gates. At this point, the probability of the disentangler removing such a region scales $\propto \exp(-l)$. Whereas, the probability of the entangler to grow this region to length $l+1$ in a maximally entangled manner scales $\propto l$. Therefore, given enough time, there is a finite probability that a highly entangled region is created with a sufficient length that it is more likely to grow than shrink. Such a region will then proliferate and the system will eventually have extensive, volume law entanglement. In other words, in the thermodynamic limit, the entangler will eventually always win for any $p < 1$. Since the time required to randomly generate an entangled region of length l is exponential in $1/(1-p)$, this argument also explains the exponential in $1/(1-p)$ relaxation time observed in Fig. 5c.

V. DISCUSSION

Inspired by measurement-induced phase transitions, we introduced a new playground for quantum random circuits in which disentangling measurements are replaced by dynamically chosen unitary gates that minimize the entanglement utilizing limited knowledge about the state. We investigated three different variants of the model: a classical surface growth model, a Clifford circuit, and a circuit with generic $U(4)$ gates. For the classical and Clifford cases, we found a phase transition between a volume law and an area law phase, with a critical point where the entanglement entropy (or height, in the classical case) increases as the square root of the system size. We could gain a deeper understanding of the classical model by comparing it to a stochastic Fredkin spin chain. Regarding the Clifford circuit, we found a qualitative behavior very similar to the classical one. However, the numerical limitations in system size did not allow us to determine whether the transition belongs to the same universality class with certainty. In the model with random Haar unitaries, we found a qualitatively different behavior: we did not observe a phase transition between volume law and area law for any finite disentangler probability $p < 1$. Instead, we found that the steady state is maximally entangled for any $p < 1$ as $L \rightarrow \infty$. We provided a heuristic argument for this behavior based on the inefficiency of the disentangler to remove multipartite entanglement.

The framework of the unitary circuit game opens many exciting directions for future research in random circuits. To begin with, going beyond the classical model, it is unclear to which different universality classes the transitions belong to. The phase transitions found in the classical and Clifford models have shown to have very similar critical behavior. However, further investigation are required to determine whether both transitions actually belong to the same universality class. Another exciting avenue for exploration is to consider different variations of the game, either changing the rules or by restricting the gates to different subsets of $U(4)$ —which is expected to lead to different behavior. Additionally, our current work employs a disentangler that minimizes the entanglement entropy on a bond, but this strategy does not facilitate a transition in the case with generic $U(4)$ unitaries for any finite rate of disentangling. It remains an open question whether optimizing other quantities could allow for an efficient control of entanglement growth in the thermodynamic limit. Lastly, the possibility of experimental measurement of Rényi entanglement entropies [41–43] raises the exciting prospect of implementing the entangling game on physical hardware.

ACKNOWLEDGMENTS

We are grateful to Adam Nahum and Curt von Keyserlingk for insightful discussions. We are grateful to Luke Causer for insightful discussions and for sharing

data for the stochastic Fredkin chain. This research was financially supported by the European Research Council (ERC) under the European Union’s Horizon 2020 research and innovation program under grant agreement No. 771537. A.S. acknowledges support from a research fellowship from the The Royal Commission for the Exhibition of 1851. F.P. acknowledges the support of the Deutsche Forschungsgemeinschaft (DFG, German Research Foundation) under Germany’s Excellence Strategy EXC-2111-390814868. F.P.’s research is part of the Munich Quantum Valley, which is supported by the Bavarian state government with funds from the Hightech Agenda Bayern Plus.

Data and materials availability: Raw data and simulation codes are available in Zenodo upon reasonable request [44].

Appendix A: Comparison of Clifford disentanglers

As mentioned in the main text, the Clifford disentangler has several options to maximally disentangle a bond, since there are different Clifford gates that reduce the entanglement by the same amount. Here, we compare different ways to choose the disentangling and show that they are all equivalent. This indicates that the average trajectory does not depend on which disentangling unitary is selected as long as it maximally disentangles the bond. We compare the following methods: (i) Random sampling, which checks the action of all Clifford unitaries in the given bond and chooses randomly a gate among the ones that disentangle it maximally. (ii) Reduced random sampling, which uses a reduced set of 19 Clifford unitaries that are enough to disentangle any possible bond and tries all of them out. Then, it chooses a random gate among the optimal ones. (iii) Ordered sampling, which uses the same subset of the previous method, but the chosen unitary is the first that is found to disentangle the bond maximally (so that not all unitaries are necessarily tried out).

The time evolution of the half-chain entanglement entropy for system size $L = 64$ is illustrated in Fig. 7, where the three distinct sampling methods for different disentangling probabilities are compared. Each line represents the average of 10^3 circuit realizations. Notably, all three methods yield identical results for the evolution of the entanglement entropy and the steady state value. Therefore, in our simulations we use the ordered sampling method to disentangle bonds, since it requires the least number of tries to find the disentangling gate, allowing for faster simulations.

Appendix B: Disentangling maximally entangled states

The task of the von Neumann disentangler is to find the optimal unitary in $U(4)$ that maximally minimizes

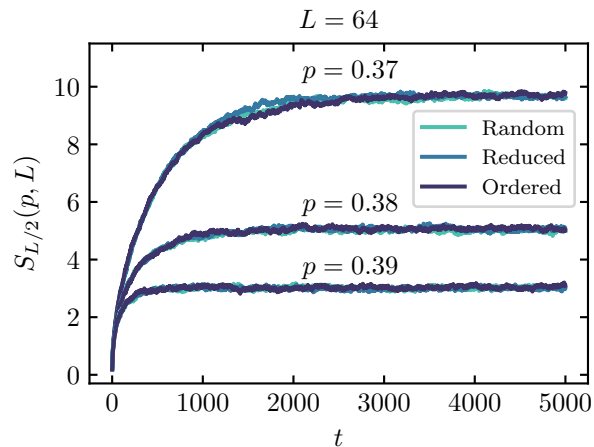


FIG. 7. Comparison of the time evolution of the half-chain entanglement entropy for different Clifford disentangler and different values of the disentangler probability for system size $L = 64$. Circuit average with 10^2 realizations.

the bipartite entanglement on a given bond. This means that it has to perform a minimization over 16 continuous parameters. Here, we investigate how effective the disentangler is when trying to disentangle a state of L qubits generated by a random circuit of depth $2L$, which is maximally entangled.

Figure 8 shows the averaged time evolution of the half-chain entanglement entropy for a disentangling circuit.

The time it takes to disentangle grows exponentially with system size. When looking at the behavior of the $L = 16$ line, we observe that the evolution gets stuck in the maximally entangled state for a long time before being able to effectively reduce the entanglement. We attribute this behavior to numerical instabilities, where the optimization fails to find the global minimum of the entanglement entropy.

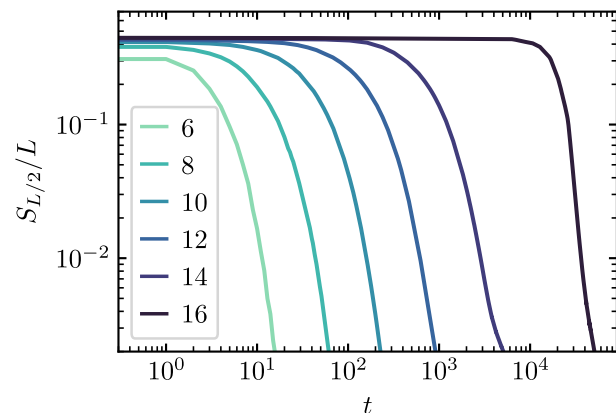


FIG. 8. Time evolution of the half-chain entanglement entropy for a disentangling circuit, with von Neumann disentangler, starting with an L -qubit state generated by a depth $2L$ random circuit. Circuit averaged over 10^2 realizations.

-
- [1] D. Basko, I. Aleiner, and B. Altshuler, Metal-insulator transition in a weakly interacting many-electron system with localized single-particle states, *Annals of Physics* **321**, 1126 (2006).
 - [2] A. Pal and D. A. Huse, Many-body localization phase transition, *Phys. Rev. B* **82**, 174411 (2010).
 - [3] R. Nandkishore and D. A. Huse, Many-body localization and thermalization in quantum statistical mechanics, *Annual Review of Condensed Matter Physics* **6**, 15 (2015).
 - [4] D. A. Abanin, E. Altman, I. Bloch, and M. Serbyn, Colloquium: Many-body localization, thermalization, and entanglement, *Rev. Mod. Phys.* **91**, 021001 (2019).
 - [5] W. D. Roeck and J. Z. Imbrie, Many-body localization: stability and instability, *Philosophical Transactions of the Royal Society A: Mathematical, Physical and Engineering Sciences* **375**, 20160422 (2017).
 - [6] F. Alet and N. Laflorencie, Many-body localization: An introduction and selected topics, *Comptes Rendus Physique* **19**, 498 (2018).
 - [7] C. J. Turner, A. A. Michailidis, D. A. Abanin, M. Serbyn, and Z. Papić, Weak ergodicity breaking from quantum many-body scars, *Nature Physics* **14**, 745 (2018).
 - [8] C. J. Turner, A. A. Michailidis, D. A. Abanin, M. Serbyn, and Z. Papić, Quantum scarred eigenstates in a rydberg atom chain: Entanglement, breakdown of thermalization, and stability to perturbations, *Phys. Rev. B* **98**, 155134 (2018).
 - [9] M. Serbyn, D. A. Abanin, and Z. Papić, Quantum many-body scars and weak breaking of ergodicity, *Nature Physics* **17**, 675 (2021).
 - [10] A. Chandran, T. Iadecola, V. Khemani, and R. Moessner, *Quantum many-body scars: A quasiparticle perspective* (2022).
 - [11] F. Wilczek, Quantum time crystals, *Phys. Rev. Lett.* **109**, 160401 (2012).
 - [12] H. Watanabe and M. Oshikawa, Absence of quantum time crystals, *Phys. Rev. Lett.* **114**, 251603 (2015).
 - [13] V. Khemani, A. Lazarides, R. Moessner, and S. L. Sondhi, Phase structure of driven quantum systems, *Phys. Rev. Lett.* **116**, 250401 (2016).
 - [14] D. V. Else, B. Bauer, and C. Nayak, Floquet time crystals, *Phys. Rev. Lett.* **117**, 090402 (2016).
 - [15] C. W. von Keyserlingk, V. Khemani, and S. L. Sondhi, Absolute stability and spatiotemporal long-range order in floquet systems, *Phys. Rev. B* **94**, 085112 (2016).
 - [16] K. Sacha and J. Zakrzewski, Time crystals: a review, *Reports on Progress in Physics* **81**, 016401 (2017).
 - [17] V. Khemani, R. Moessner, and S. L. Sondhi, *A brief history of time crystals* (2019).
 - [18] Y. Li, X. Chen, and M. P. A. Fisher, Quantum zeno effect and the many-body entanglement transition, *Phys. Rev. B* **98**, 205136 (2018).

- [19] A. Chan, R. M. Nandkishore, M. Pretko, and G. Smith, Unitary-projective entanglement dynamics, *Phys. Rev. B* **99**, 224307 (2019).
- [20] B. Skinner, J. Ruhman, and A. Nahum, Measurement-induced phase transitions in the dynamics of entanglement, *Phys. Rev. X* **9**, 031009 (2019).
- [21] Y. Li, X. Chen, and M. P. A. Fisher, Measurement-driven entanglement transition in hybrid quantum circuits, *Phys. Rev. B* **100**, 134306 (2019).
- [22] A. Zabalo, M. J. Gullans, J. H. Wilson, S. Gopalakrishnan, D. A. Huse, and J. H. Pixley, Critical properties of the measurement-induced transition in random quantum circuits, *Phys. Rev. B* **101**, 060301 (2020).
- [23] A. Lavasani, Y. Alavirad, and M. Barkeshli, Measurement-induced topological entanglement transitions in symmetric random quantum circuits, *Nature Physics* **17**, 342–347 (2021).
- [24] S. Sang and T. H. Hsieh, Measurement-protected quantum phases, *Phys. Rev. Research* **3**, 023200 (2021).
- [25] A. Lavasani, Y. Alavirad, and M. Barkeshli, Topological order and criticality in $(2 + 1)$ D monitored random quantum circuits, *Phys. Rev. Lett.* **127**, 235701 (2021).
- [26] K. Klocke and M. Buchhold, Topological order and entanglement dynamics in the measurement-only xxx quantum code, *Phys. Rev. B* **106**, 104307 (2022).
- [27] A. Lavasani, Z.-X. Luo, and S. Vijay, *Monitored quantum dynamics and the kitaev spin liquid* (2022).
- [28] A. Nahum, J. Ruhman, S. Vijay, and J. Haah, Quantum entanglement growth under random unitary dynamics, *Phys. Rev. X* **7**, 031016 (2017).
- [29] L. Causer, J. P. Garrahan, and A. Lamacraft, Slow dynamics and large deviations in classical stochastic fredkin chains, *Physical Review E* **106**, 10.1103/physreve.106.014128 (2022).
- [30] R. Movassagh and P. W. Shor, Supercritical entanglement in local systems: Counterexample to the area law for quantum matter, *Proceedings of the National Academy of Sciences* **113**, 13278 (2016).
- [31] O. Salberger and V. Korepin, Fredkin spin chain (2016), [arXiv:1605.03842 \[quant-ph\]](https://arxiv.org/abs/1605.03842).
- [32] L. Dell’Anna, O. Salberger, L. Barbiero, A. Trombettoni, and V. E. Korepin, Violation of cluster decomposition and absence of light cones in local integer and half-integer spin chains, *Phys. Rev. B* **94**, 155140 (2016).
- [33] R. Movassagh, The gap of fredkin quantum spin chain is polynomially small, *Annals of Mathematical Sciences and Applications* **3**, 531 (2018).
- [34] X. Chen, E. Fradkin, and W. Witczak-Krempa, Gapless quantum spin chains: multiple dynamics and conformal wavefunctions, *Journal of Physics A: Mathematical and Theoretical* **50**, 464002 (2017).
- [35] Clifford gates are unitaries that transform Pauli string operators into Pauli string operators.
- [36] D. Gottesman, Class of quantum error-correcting codes saturating the quantum hamming bound, *Phys. Rev. A* **54**, 1862 (1996).
- [37] D. Gottesman, The heisenberg representation of quantum computers (1998), [arXiv:quant-ph/9807006 \[quant-ph\]](https://arxiv.org/abs/quant-ph/9807006).
- [38] D. Gottesman, Stabilizer codes and quantum error correction (1997), [arXiv:quant-ph/9705052 \[quant-ph\]](https://arxiv.org/abs/quant-ph/9705052).
- [39] S. Aaronson and D. Gottesman, Improved simulation of stabilizer circuits, *Phys. Rev. A* **70**, 052328 (2004).
- [40] We can also consider a Rényi disentangler, that minimizes the bipartite n -th Rényi entropy across the bond. Our numerical results for such disentanglers with $n > 1$ show an equivalent behavior to the von Neumann disentangler.
- [41] R. Islam, R. Ma, P. M. Preiss, M. E. Tai, A. Lukin, M. Rispoli, and M. Greiner, Measuring entanglement entropy in a quantum many-body system, *Nature* **528**, 77 (2015).
- [42] H. Pichler, G. Zhu, A. Seif, P. Zoller, and M. Hafezi, Measurement protocol for the entanglement spectrum of cold atoms, *Phys. Rev. X* **6**, 041033 (2016).
- [43] A. M. Kaufman, M. E. Tai, A. Lukin, M. Rispoli, R. Schittko, P. M. Preiss, and M. Greiner, Quantum thermalization through entanglement in an isolated many-body system, *Science* **353**, 794 (2016), <https://www.science.org/doi/pdf/10.1126/science.aaf6725>.
- [44] R. Morral-Yepes, A. Smith, S. L. Shondi, and F. Pollmann, *Entanglement transitions in unitary circuit games* (2023).